Section 2 Plasma Physics

Chapter 1. Plasma Dynamics

Academic and Research Staff

Professor George Bekefi, Professor Abraham Bers, Professor Bruno Coppi, Professor Miklos Porkolab, Professor Jonathan S. Wurtele, Dr. Kuo-in Chen, Dr. Shien-Chi Chen, Dr. Thomas Dupree, Dr. Ronald C. Englade, Dr. Stanley C. Luckhardt, Dr. Stefano Migliuolo, Dr. Abhay K. Ram, Dr. Linda Sugiyama, Ivan Mastovsky

Visiting Scientists

Paolo Detragiache,[1] Vladimir Fuchs,[2] Lazar Friedland,[3] Dr. Chaim Leibovitch,[4] Dr. Kongyi Xu[5]

Graduate Students

Ala Alryyes, Ricardo Betti, Carson Chow, Stefano Coda, Jeffrey A. Colborn, Manoel E. Conde, Christian E. de Graff, Anthony C. DiRienzo, Robert J. Kirkwood, Kenneth C. Kupfer, Yi-Kang Pu, Jared P. Squire, Richard E. Stoner, Jesus N.S. Villasenor

Undergraduate Students

Daniel P. Aalberts, George Chen, Salvatore DiCecca, Marc Kaufman, Weng-Yew Ko, Nora Nerses, Kurt A. Schroder

1.1 Relativistic Electron Beams

Sponsors

Lawrence Livermore National Laboratory
(Subcontract 6264005)
National Science Foundation
(Grants ECS 84-13173 and ECS 85-14517)
U.S. Air Force - Office of Scientifc Research
(Contract AFOSR 84-0026)
U.S. Army - Harry Diamond Laboratories
(Contract DAAL02-86-C-0050)
U.S. Navy - Office of Naval Research
(Contract N00014-87-K-2001)

Project Staff

Professor George Bekefi, Professor Jonathan S. Wurtele, Manoel E. Conde, Christian E. de Graff, Richard E. Stoner, Anthony C. DiRienzo, Daniel P. Aalberts, Salvatore DiCecca, Dr. Kongyi Xu, Dr. Chaim Leibovitch, Ivan Mastovsky, Dr. Shien-Chi Chen

1.1.1 Coherent, Free-Electron Radiation Sources

The primary objective of the group is to develop a basic experimental and theoretical understanding of coherent generation by free electrons for wavelengths in the 1 μm to 10 cm range. Particular emphasis is placed on free electron lasers, Cerenkov sources, rel-

---

[1] University of Turin, Torino, Italy.

[2] IREQ, Quebec, Canada.

[3] Hebrew University of Jerusalem, Israel.

[4] Rafael Laboratory, Haifa, Israel.

[5] China University of Electronic Science and Technology, Chengdu, People's Republic of China.

ativistic magnetrons, and other novel radiation sources.

The experiments are carried out on four high-voltage pulsed accelerators available in our laboratory. Their characteristics are summarized in table 1.

Table 1. High-Voltage Pulsed Accelerators.

Accelerator	Voltage	Current	Pulse Length	Repitition Range
Physics International Pulserad 110A	1.5 MV	20 kA	30 nsec	n/a
Nereus Accelerator	600 kV	150 kA	30 nsec	n/a
Physics International 615MR Pulserad	500 kV	4 kA	1μ sec	n/a
High Voltage Modulator	700 kV	600 A	1μ sec	1 pps

During the past year, work has been carried out in the following areas.

Observations of Field Profile Modifications in a Raman Free Electron Laser Amplifier

Free electron laser (FEL) amplification is the consequence of a resonant interaction between an incident electromagnetic wave and a co-propagating electron beam that has been injected into a periodic "wiggler" magnetic field. This can lead to high output gain, and high efficiency of converting electron beam kinetic energy into radiation. Remarkably, it also leads to large phase shifts in the amplified electromagnetic wave. Under proper circumstances this phase shift can have a sign such that the electromagnetic wave is refracted towards the axis of the electron beam in a manner somewhat akin to the guiding properties of an optical fiber. Such "optical guiding" would mitigate the effects of diffraction, and thereby allow the length of FEL wigglers to exceed the Rayleigh range. Long wigglers are needed if free electron lasers are to operate either in the vacuum-ultraviolet or at high efficiencies in the infrared wavelength regime.

It comes as no surprise that strong FEL activity as described above should be accompanied by significant modification of the spatial distribution of the RF fields within and in the immediate vicinity of the electron beam. To be sure, one way of confirming optical guiding is by observation of the changes in the transverse spatial profile of the co-propagating amplified wave. Such field probing can be quite difficult at short wavelengths (infrared and visible). However, the microwave regime, in which our experiments are conducted, offers a relatively simple and direct way. We allow small, movable electric dipole antennas to traverse the waveguide in which the interaction takes place. Using antennas sensitive to different polarizations, we are then able to distinguish between wave types.[6]

Tunable Micro-Wigglers for Free Electron Lasers

Short period (1-10 mm) wigglers for free electron laser applications have been a subject of considerable interest. Besides their compactness, such systems have the advantage of producing higher frequency radiation with a given electron energy, or conversely, they reduce the electron energy required to access a given wavelength.

The wigglers proposed in previous works lack a simple but precise field tuning mechanism so important in numerous applications. We have constructed[7] a novel micro-wiggler with this unique flexibility. The 30-period micro-wiggler, with a periodicity of 2.4 mm, is shown in figure 1a. The wiggler consists

---

[6] F. Hartemann, K. Xu, G. Bekefi, J.S. Wurtele, and J. Fajans, "Wave Profile (Optical Guiding) Induced by the Free Electron Laser Interaction," *Phys. Rev. Lett.* 59(11):1177 (1987); K. Xu, G. Bekefi, and C. Leibovitch, "Observations of Field Profile Modifications in a Raman Free Electron Laser Amplifier," submitted to *Phys. Fluids* (1989).

[7] S-C. Chen, G. Bekefi, S. DiCecca, and R. Temkin, "Tunable Micro-Wigglers for Free Electron Lasers," submitted to *Appl. Phys. Lett.* 54:1299 (1989).

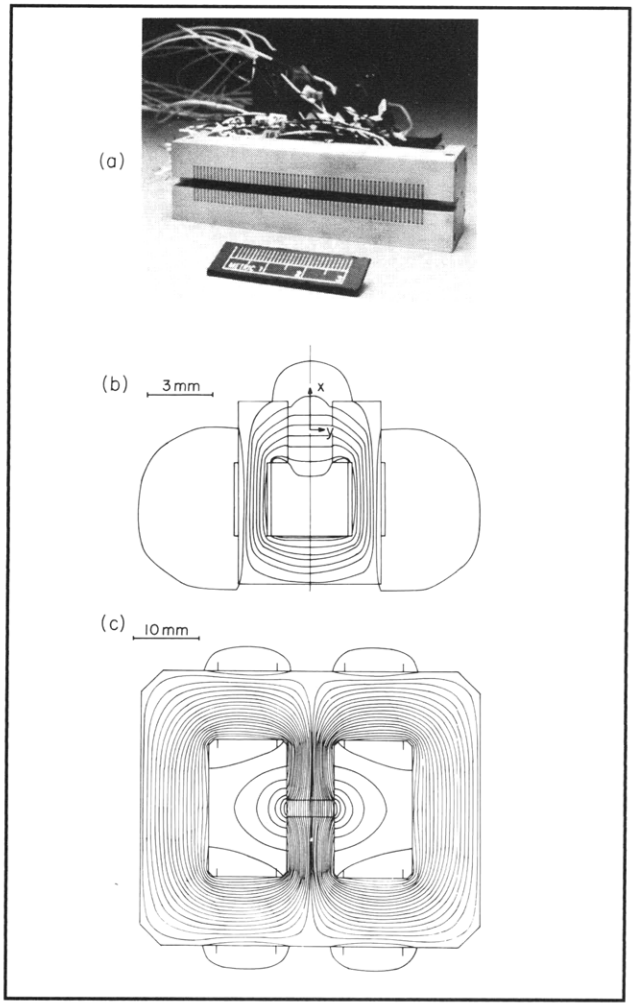

Figure 1. Microwigglers for free electron laser applications.

of a periodic assembly of tiny electromagnets each of which is energized by its own current windings (see figure 1b). The magnetic field in each half-period is independently controllable and the experimentally demonstrated tunability provides a versatile means for achieving the wiggler field required for optimal FEL operation, such as reduction of random field errors, field tapering, optical klystron configurations, and electron beam matching at the wiggler entrance. The measured operating characteristics of the microwiggler in the linear regime (that is, well below saturation of the magnet material) agree very well with both analytical predictions and numerical models. The saturation behavior in the magnet structure is also studied experimentally and by nonlinear finite element simulations.

An alternate and better design under consideration is shown in figure 1c.

Effects of Electron Prebunching on the Radiation Growth Rate of a Collective (RAMAN) Free-Electron Laser

The concept of prebunching electron beams has a long and venerable history; the klystron is a famous example. Prebunching is also used to improve the performance of other sources of coherent radiation. It is used in traveling wave tubes (TWT) to suppress parasitic feedback oscillations caused by wave reflections at or near the output of the device, and it has been used in traveling wave tubes and klystrons to achieve radiation at high frequencies by arranging for the bunched beam to emit on high harmonics. In more recent applications, prebunching the beams in gyrotrons (the so-called gyroklystron configuration) can lead to improved efficiency. In the case of free electron lasers (FEL's), systems with prebunching are referred to as optical klystrons. The concept has been employed successfully to increase the overall optical gain both at the fundamental and at high harmonics. Such gain enhancement is of particular importance at short wavelengths (visible and VUV) where FEL gains are of necessity small.

To date, experimental and theoretical studies of the optical klystron have been carried out in the low gain, single particle (Compton) regime applicable to very short radiation wavelengths (visible and ultraviolet) where electron beam energies in excess of several hundred MeV are used. In contrast, our experiments are made at microwave frequencies using mildly relativistic electrons (~200 keV). In this collective (Raman) regime, the gains are high and the effects of space charge cannot be neglected. We find[8] that

[8] C. Leibovitch, K. Xu, and G. Bekefi, "Effects of Electron Prebunching on the Radiation Growth Rate of a Collective (Raman) Free Electron Laser Amplifier," *IEEE J. Quantum Elect.* 24:1825 (1988); J.S. Wurtele, G. Bekefi, R. Chu, and K. Xu, "Prebunching in a Collective Raman Free Electron Laser Amplifier," submitted to *Phys. Fluids* (1989).

prebunching does indeed increase the growth rate of the radiation quite dramatically as compared with the case where prebunching has not been incorporated.

A 35 GHz Cyclotrom Autoresonance Maser Amplifier

The cyclotron autoresonance maser (CARM) has been subjected to extensive theoretical studies and numerical simulations. However, unlike the gyrotron and the free electron laser, its capabilities as a source of coherent millimeter wavelength radiation remain virtually untested in the laboratory. To the best of our knowledge, only CARM oscillator experiments have been reported in the literature.

Figure 2 illustrates what we believe to be the first CARM amplifier experiment.[9] We have measured a small signal gain of 90 dB/m and a saturated RF power of 10 MW in the frequency band of 35±1 GHz. The electronic efficiency of converting electron beam energy to radiation is 3 percent.

1.2 Plasma Wave Interactions — RF Heating and Current Generation

Sponsors

U.S. Department of Energy
(Contract DE-AC02-78-ET-51013)
National Science Foundation
(Grant ECS 85-15032)

Project Staff

Professor Abraham Bers, Dr. Abhay K. Ram, Ala Alryyes, George Chen, Carson Chow, Lazar Friedland, Vladimir Fuchs, Weng-Yew Ko, and Kenneth C. Kupfer

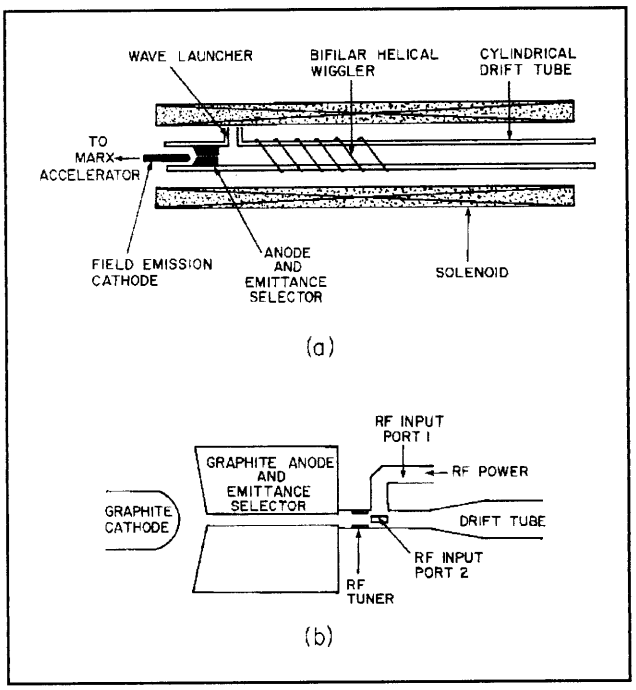

Figure 2. a) Schematic of a cyclotron autoresonance maser amplifier; b) Detail of the RF launcher.

1.2.1 Introduction

An overall description of the work of this group was given in Progress Report Number 130.

Our work of the past year has focused on two aspects:

1. Diffusion in transport induced by coherent waves in plasmas; this work extends our nonlinear studies of induced stochasticity and chaos to coupling velocity and configuration space dynamics. It is reported in sections 1.2.2, "Spatial Stochasticity Induced by Coherent Wavepackets" on page 159 and 1.2.3, "Transport in RF Heating and Current Drive" on page 160.

2. Kinetic wave propagation and mode conversion in magnetized plasmas; this work entails extending ray tracing to kinetic descriptions of plasmas in complex magnetic configurations, and developing reduced-order analyses at singular layers

[9] G. Bekefi, A. DiRienzo, C. Leibovitch, and B.G. Danly, "A 35 GHz Cyclotron Autoresonance Maser Amplifier," submitted to *Appl. Phys. Lett.* 54:1302 (1989); A.C. DiRienzo, G. Bekefi, C. Leibovitch, and B.G. Danly, "Radiation Measurements from a 35 GHz Cyclotron Autoresonance (CARM) Amplifier," *SPIE* (1988).

in such plasmas. This work is described in sections 1.2.4, "Kinetic Ray Tracing Code — Phase and Amplitude" on page 163 and 1.2.5, "Reduced-Order Analyses for Ion Cyclotron Heating*" on page 164.

1.2.2 Spatial Stochasticity Induced by Coherent Wavepackets

As a first step towards the understanding of particle transport induced by RF waves, it is necessary to know the phase-space behavior of those particles that interact with the coherent field spectrum. In particular, we are interested in the phase-space behavior of charged particles moving in one-dimensional configuration space (along the magnetic field lines) and interacting periodically with an electrostatic wave. Such a situation would represent the interaction of tail electrons with a lower hybrid wave. Towards this end, we have developed and analyzed a model for the periodic interaction of charged particles with a spatially localized (delta-function), time-dependent electrostatic force.[10] The (normalized) equations of motion are:

$$\frac{dv}{dt} = \varepsilon \cos(2\pi t) \sum_{n=-\infty}^{\infty} \delta(z-n) \qquad (1)$$

where ε is the field strength of the electrostatic wave, v is the velocity and dz/dt = v. This system lends itself to an extensive analytical and numerical analysis primarily because the mapping equations (representing the change in the energy of the particles after each interaction with the impulsive force) can be explicitly derived. The mapping equations are:

$$u_{n+1} = u_n + 2\sigma\varepsilon \cos 2\pi t_n \qquad (2)$$

$$t_{n+1} = t_n + \frac{1}{\sqrt{u_{n+1}}} \mod 1 \qquad (3)$$

where u_{n+1} is the energy of the particle after it has received its n-th impulse and t_{n+1} is the time (or the phase of the wave) at which it arrives at the position where it receives its (n+1)-th impulse; σ is either 1, or 0, or -1 and is related to the direction of the velocity of the particle. These mapping equations have been extensively analyzed to determine the conditions under which the motion of the charged particles becomes chaotic and the domain of phase-space that becomes chaotic.[11]

One of the features of this map is that the chaotic phase-space is always finite for any finite amplitude, ε. This will be the generic behavior of all charged particles interacting periodically with any spatially imposed coherent field. In other words, boundedness

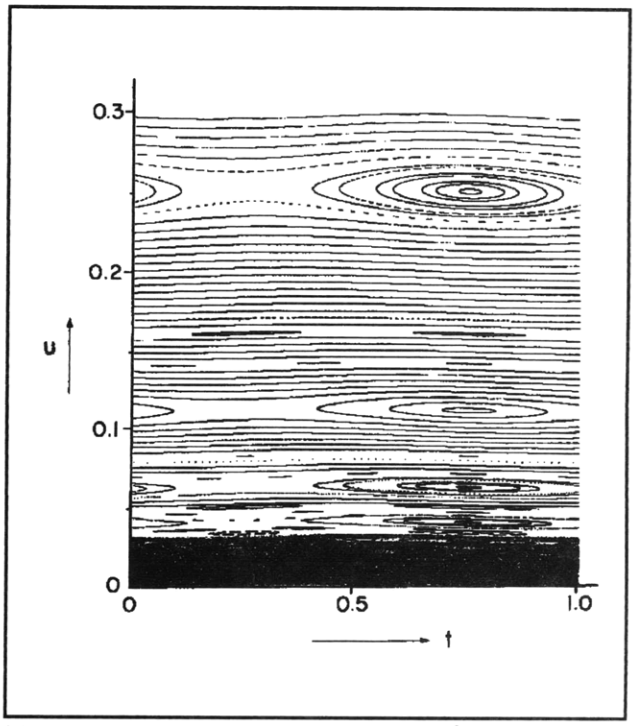

Figure 3. Phase-space plot for $\varepsilon = 10^{-3}$.

[10] A.K. Ram, A. Bers, and K. Kupfer, *Periodic Interactions of Charged Particles with Spatially Localized Fields.* Plasma Fusion Center Report, PFC/JA-88-41. MIT, 1988 (accepted for publication in *Phys. Lett. A*); A.K. Ram, A. Bers, and K. Kupfer, "The 'Spatial' Standard Map," *Bull. Am. Phys. Soc.* 33:1877 (1988).

[11] Ibid.

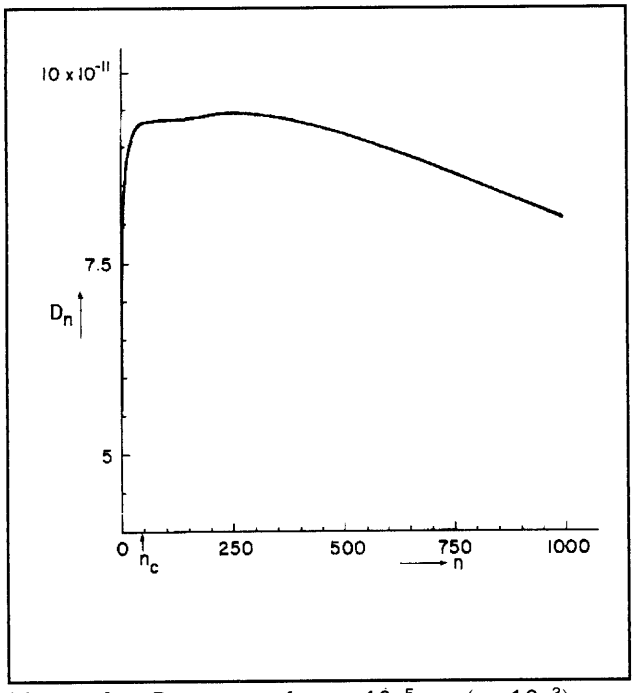

Figure 4a. D_n versus n for $\varepsilon = 10^{-5} < \varepsilon_c (\varepsilon_c \approx 10^{-3})$.

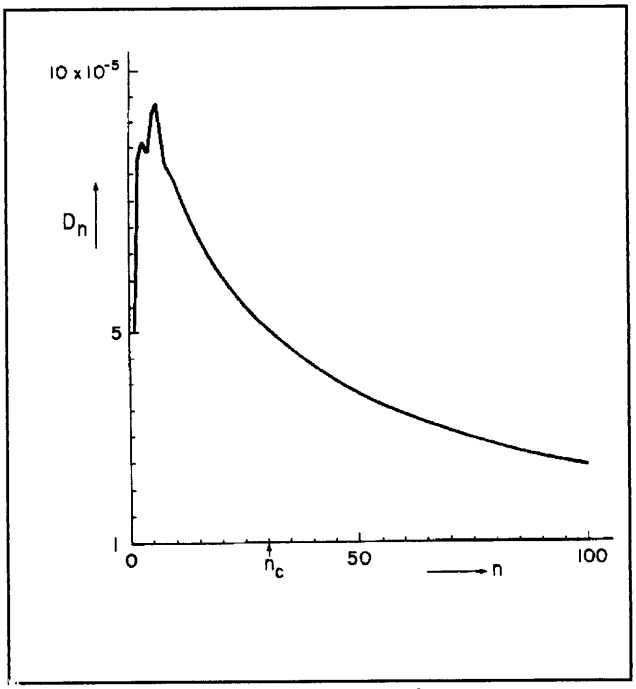

Figure 4b. D_n versus n for $\varepsilon = 10^{-2} > \varepsilon_c$. n_c indicates the value of n beyond which correlations have decayed to zero.

of the chaotic phase-space will occur in any physical situation of the type described above. Under these circumstances a distribution of particles in the chaotic phase-space will not diffuse forever. If we define:

$$D_n = \frac{1}{2n} <(u_n - u_o)^2>$$

where <...> denotes ensemble average over a set of initial conditions with energy u_o distributed randomly in t, then in the limit $n \to \infty$, for a bounded region of stochasticity $D_n \to 0$. (In an unbounded or periodic stochastic phase-space the limit $n \to \infty$ would give the conventional diffusion coefficient.) It is important to know the diffusion coefficient so that the evolution of the distribution function of particles can be described by the Fokker-Planck description. By a detailed study of the mapping equations, we find that the concept of diffusion can be used to describe the dynamics in the stochastic region only for amplitudes below a certain critical amplitude. The critical amplitude is determined by the width of the stochastic region and the correlation time. At the critical amplitude within a correlation time a majority of the particles in a beam will have reached the boundaries of the stochastic region. For amplitudes above the critical amplitude, the dynamics do not seem to be described by the usual concept of diffusion. In this case, even though the distribution function may have evolved to a steady state, its evolution to that state may not be described by the Fokker-Planck equation.

1.2.3 Transport in RF Heating and Current Drive

We are investigating the effects of coherent RF wave-fields on the transport of particles. This is in contrast to usual transport analyses which assume that the fields are of random phase.[12] If one assumes that the fields are coherent, then the random phase assumption inherent in the previous analyses is of questionable validity. For example, it has been shown that correlations in two-dimensional

[12] A.N. Kaufman, *Phys. Fluids* 15:1063 (1972); H.E. Mynick. Princeton University Plasma Physics Laboratory Report No. PPPL-2534. Princeton, New Jersey: 1988.

hamiltonian chaos drive the local diffusion coefficient into oscillations about the random phase value;[13] such models have been proposed for studying the velocity space diffusion of tail particles in an RF heated plasmas.[14] We are extending these studies by coupling the chaos in velocity space to configuration space, thereby obtaining the spatial transport of particles across flux surfaces.

In developing this problem, we have considered the following simplified model of superthermal electrons. The field structure is considered localized on a flux surface where electrons cycle through it periodically. An electron's interaction with the field on each transit is taken to be

$$\frac{dz}{dt} = v \tag{1}$$

$$\frac{dv}{dt} = \alpha e^{-z^2/d^2}\cos(z-t), \tag{2}$$

where $\alpha = (eE_{\|}k/m\omega^2)$ is the normalized field strength, d specifies the width of the interaction region, and v is the parallel velocity of the particle; distance is normalized to the wave-number k and time to the frequency ω. The electron's radial guiding center drift is simply

$$\frac{dr}{dt} = (v^2+v_{\perp}^2/2)\frac{2\pi}{L}\sin(\frac{2\pi z}{L}+\theta_0), \tag{3}$$

where the radial position, r, is normalized to ρ_0,

$$\rho_0 = (\frac{\omega}{k\omega_{ce}})(\frac{L}{2\pi R_0}),$$

L is the normalized path length along one poloidal circuit of the field line, and θ_0 is the poloidal angle about which the wave-packet is localized. In this approximation, the electron's perpendicular velocity, $v_{\perp}$, is conserved. Note that equation (3) ignores the perpendicular RF fields which also contribute to radial motion.

If after an electron's n^{th} transit through the wave-packet, the time is t_n and the parallel velocity is v_n, then integrating equations (1) and (2) in z from $-L/2$ to $L/2$ give the values of t_{n+1} and v_{n+1}. This mapping can be iterated for a given initial condition (t_0,v_0) and plotted in the appropriate surface of section. For example, the map is area preserving when v_n^2 is plotted against t_n(modulus 2π). When $L\alpha d>4$, the map contains a connected region of stochasticity, bounded in parallel velocity by two KAM surfaces on either side of the resonance at $v = 1$. For $\alpha d \ll 1$ and $L \gg d$, these KAM surfaces are accurately located by the two values of v for which $K(v) = 1$,

$$K(v) \equiv (\frac{L\alpha d\sqrt{\pi}}{v^3})e^{-(1-\frac{1}{v})^2 d^2/4} \tag{4}$$

where K(v) is the local standard map parameter.[15] Large primary islands are embedded in the upper portion of the stochastic phase space where K dips below 4 so that the first order fixed points are elliptic.

The radial motion is obtained by integrating equation (3) as the electron transits the wave-packet and its parallel velocity fluctuates. In general, as an electron diffuses in the stochastic region of parallel phase space it also diffuses radially. The radial diffusion is found to be extremely sensitive to the localization of the fields; field structures extending over a broad range of poloidal angles diffuse the particles across flux surfaces at a much faster rate. This effect can be visualized by allowing the field envelope on the right-hand side of equation (2) to

---

[13] A.J. Lichtenberg and M.A. Lieberman. University of California at Berkeley Report No. UCB/ERL M88/5. Berkeley, California: 1988; A.K. Ram, A. Bers, and K. Kupfer. MIT Plasma Fusion Center Report No. PFC/JA-88-41. MIT, 1988.

[14] V. Fuchs, V. Krapchev, A. Ram, and A. Bers, *Physica* 14D:141 (1985); S.J. Tanaka, *Plasma Phys. Contr. Fusion* 29-9:067 (1987).

[15] V. Fuchs, V. Krapchev, A. Ram, and A. Bers, *Physica* 14D:141 (1985).

become a delta-function. In this case, the radial equation is easy to integrate and one finds that

$$\Delta r_N = \sum_{n=1}^{N} \Delta v_n \cos \theta_n \, . \qquad (5)$$

Δr_N is the change in average radial position resulting from N instantaneous jumps in parallel velocity, where the n^{th} jump, Δv_n, occurs at the poloidal angle θ_n. Note that we ignored $v^2/2$ compared to v^2 when integrating equation (3) to obtain equation (5) in this particularly simple form; retaining this term does not affect the following argument. If all the impulsive kicks occur at the same poloidal angle, then $\cos \theta_n$ can be pulled out of the sum in equation (5). The remaining sum is simply $v_N - v_0$, which is bounded as $N \to \infty$ because the stochastic orbits cannot diffuse past the last KAM surface in parallel phase space. Thus an electron being scattered in an infinitely narrow range of poloidal angle remains within a scale length ρ_0 of its initial radial position so that there is no radial diffusion. On the other hand, if the impulsive kicks occur at two or more values of θ_n, then the sum in equation (5) is not bounded and one has the following equation for radial diffusion

$$\lim_{N \to \infty} <\Delta r_N^2>/N = \eta \overline{D}, \qquad (6)$$

where $<\ >$ denote an ensemble average over an even distribution of initial conditions in the stochastic phase space, $\overline{D}$ is the ensemble averaged diffusion coefficient in parallel velocity, and η is the average value of $\cos^2\theta$ weighted by the poloidal distribution of the field intensity. The numerical value of $\overline{D}$ and details concerning the structure of velocity space diffusion (when the field envelope is a delta-function) are given in our related work,[16] described in section 1.2.2, "Spatial Stochasticity Induced by Coherent Wavepackets" on page 159.

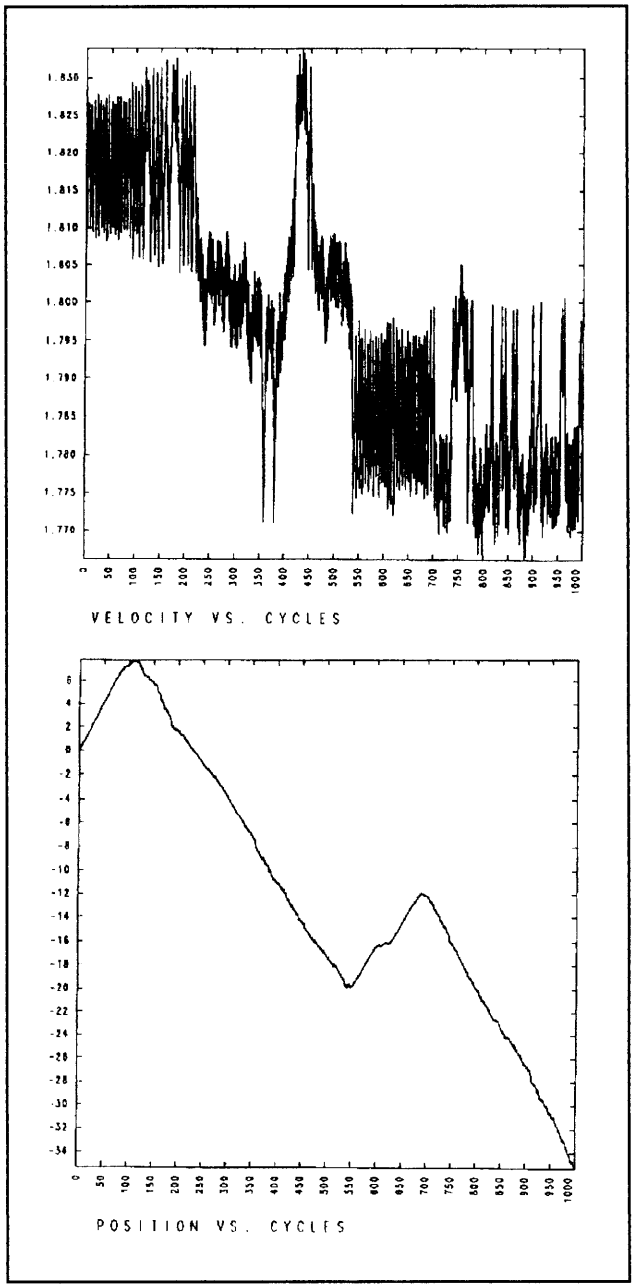

Figure 5. Parallel velocity (top figure) and the radial position (bottom) as a function of the number of transits through the wave packet. The radial position has a positive slope when the particle is in the vicinity of an island and a negative slope when it is diffusing between islands.

Finally, we have found and characterized some distinctive behavior associated with the integration of the radial drift in equation (3)

[16] A.K. Ram, A. Bers, and K. Kupfer, *Periodic Interactions of Charged Particles with Spatially Localized Fields.* Plasma Fusion Center Report, PFC/JA-88-41. MIT, 1988 (accepted for publication in *Phys. Lett. A*).

through a finite width field structure as given by our model equations (1) and (2). In particular, as stochastic orbits diffuse through the portion of phase space, where $4 > K(v) > 1$ and $v > 1$,they are convected radially. The effect is entirely due to the large primary islands embedded in this region which prevent a dynamical average of the radial jumps from vanishing. The convection scales like $(d/L)^2\rho_0$ per transit and can be inward or outward depending on the poloidal angle about which the RF field is localized.

1.2.4 Kinetic Ray Tracing Code — Phase and Amplitude

This study was motivated by experimental observations of significant electron heating when the fast Alfvén wave (FAW) in the ion-cyclotron range of frequencies is launched into tokamak plasmas. Ordinarily one assumes that the slowing down of the minority ion tail heats the electrons. However, in some recent experiments on JET, this could not entirely account for the intense electron heating observed. In simple theoretical analyses the electrons could get heated by transit-time damping of the FAW, but this was not sufficient to explain the observations. We decided to study the fate of the ion-Bernstein wave (IBW) as it propagated in a toroidal plasma to see if that could be an explanation for the observed electron heating. The IBW is a natural consequence of the mode-conversion process that occurs near the ion-ion hybrid resonance (in two-ion species plasmas). The conversion process is efficient for low $k_\parallel$'s (magnitude of the wave-vector parallel to the magnetic field) which carry significant power from single loop antennas into the plasma. To study the propagation of IBW, we developed a fully kinetic (Vlasov) ray trajectory code which followed IBWs in toroidal geometry.[17] A detailed numerical analysis revealed that the $k_\parallel$'s along the IBW upshifted rapidly as it propagated away from the mode-conversion layer. The upshift could lead to electron Landau damping. The code was for a hot Maxwellian plasma containing profiles in density, temperature, poloidal and toroidal magnetic fields. The code results were well substantiated by simple analytical models for the propagation of an IBW.[18]

Since that work, we have found that the code is general enough to be used to study the propagation of waves of any frequency in tokamaks. Furthermore, we have recently supplemented the code to calculate the amplitude of the electric field along the ray trajectory. To this end, we have to include the solution of the following differential equations:[19]

$$\frac{dU}{dt} + U\nabla \cdot \frac{\partial \omega}{\partial \vec{k}} + \hat{e}^* \cdot \bar{\bar{\sigma}}^H \cdot \hat{e} \mid \alpha \mid^2 = 0 \quad (1)$$

where

$$U = \frac{1}{8\pi} \frac{\partial(\omega\varepsilon)}{\partial\omega} \mid \alpha \mid^2 \quad (2)$$

is the energy density associated with the mode of amplitude α, and $\bar{\bar{\sigma}}^H$ is the hermitian part of the conductivity tensor. The second term in (1) describes the effect of the nearby rays on the particular ray trajectory being followed (i.e., it includes the effects of focusing), and the third term in (1) describes the damping along the ray. In order to evaluate the second term in (1) along the rays, we need to solve the following six coupled equations for dyadic, $\nabla\vec{k}$:

---

[17] A.K. Ram and A. Bers, In *Applications of Radio-Frequency Power to Plasmas.* AIP Conference Proceedings 159, eds. S. Bernabei and R.W. Motley, 402-405. New York: American Institute of Physics: 1987.

[18] Ibid.

[19] A. Bers, In *Plasma Physics - Les Houches 1972,* eds. C. DeWitt and J. Peyraud. London, Gordon & Breach Science Publishers: 1975; I.B. Bernstein and L. Friedland, In *Handbook of Plasma Physics,* eds. M.N. Rosenbluth and R.Z. Sagdeev, Vol. 1: Basic Plasma Physics I, eds. A.A. Galeev and R.N. Sudan. North-Holland Pub. Co.: 1983.

$$\frac{d(\vec{\nabla}\vec{k})}{dt} = -\frac{\partial^2\omega}{\partial\vec{r}\,\partial\vec{r}} - (\vec{\nabla}\vec{k}) \cdot \frac{\partial}{\partial\vec{k}} \frac{\partial\omega}{\partial\vec{k}}$$

$$-\left(\frac{\partial}{\partial\vec{r}} \frac{\partial\omega}{\partial\vec{k}} + (\vec{\nabla}\vec{k}) \cdot \frac{\partial^2\omega}{\partial\vec{k}\,\partial\vec{k}}\right) \cdot \vec{\nabla}\vec{k} \qquad (3)$$

Results of these calculations should be forthcoming in a future publication.

1.2.5 Reduced-Order Analyses for Ion Cyclotron Heating*

Mode Conversion in the Presence of Kinetic Dissipation

Reduced order analytic descriptions of the coupling between fast Alfvén waves (FAW) and ion-Bernstein waves (IBW) in ICH are useful for gaining insight into the scaling of such heating, and for simplifying two- and three-dimensional kinetic codes. Even in one-dimension (in the direction x of the toroidal field gradient), the FAW-IBW coupling is usually represented approximately by a fourth (or sixth) order o.d.e. derived from the Vlasov-Maxwell equations. This high-order o.d.e. must then be solved by numerical techniques. In recent work, using nonresonant (quasimode) perturbation theory,[20] we have shown that the FAW transmission coefficient (T) can be obtained in closed form from the solution of a first-order o.d.e.. These closed form, analytic results are in excellent agreement with those obtained from numerical solutions of the full fourth (or sixth)-order o.d.e. description. Also recently, we have shown that both the transmission coefficient (T) and the reflection coefficient (R) of the incident FAW can be obtained accurately from a reduced second-order o.d.e.[21] We present here the completion of the reduced analytic description by showing that the mode-conversion coefficient (C), in the presence of kinetic dissipation, can be decribed approximately by a coupled mode system of two first-order o.d.e.'s (CME's) which we solve in closed form.[22] With the knowledge of T, R, and C, the power dissipated (D) per unit of incident FAW power is obtained from global energy conservation.

We start from the usual 2 x 2, zero-electron-mass, local dispersion tensor for ICRF,[23] and expand the elements to first-order in $(k_\perp\rho_i)^2$. We thus obtain

$$N_\perp^4 K_1 + N_\perp^2(K_0 - 2\lambda K_1) - 2\lambda K_0 + \lambda^2 = 0 \quad (1)$$

where

$$\lambda = (1/3) - N_\parallel^2,\ N = kc_A/\omega,\ c_A$$

is the majority Alfvén speed,

$$K_0 = (-1/3) - N_\parallel^2 + (\eta/4N_\parallel\sqrt{\beta_2})Z(a_2\xi),$$

$$K_1 = (\sqrt{\beta_1}/4N_\parallel)Z(a_1\xi),$$

$$a_{1,2} = c_A/N_\parallel\sqrt{\beta_{1,2,}}\ R_o\omega,\ \xi = x\omega/c_A,\ R_0$$

is the tokamak major radius, 1 refers to the majority and 2 to the minority ion species. The approximate IBW dispersion relation, $\varepsilon_{xx} = n_\parallel^2$, is $K_0 + K_1N_\perp^2 = 0$, and (1) can be factored into

$$(2\lambda - N_\perp^2)(K_0 + K_1N_\perp^2) = \lambda^2. \qquad (2)$$

The corresponding wave equations for the coupled FAW and the IBW are

$$F'' + 2\lambda F = \lambda B \qquad (3a)$$

---

[20] G. Francis et al., In *Applications of Radio-Frequency Power to Plasmas.* AIP Conference Proceedings 159, eds. S. Bernabei and R. Motley, 370-373. New York, American Institute of Physics: 1987; A. Bers et al., In *Europ. Phys. Soc. Contributed Papers*, eds. F. Englemann and J.L. Alvares Rivas, Vol. 11D, Part III, pp. 995A-C. 1987.

[21] C.N. Lashmore-Davies, V. Fuchs, G. Francis, A.K. Ram, A. Bers, and L. Gauthier, *Phys. Fluids* 31:1614 (1988).

[22] V. Fuchs and A. Bers, *Phys. Fluids* 31:12 (1988).

[23] C.N. Lashmore-Davies, V. Fuchs, G. Francis, A.K. Ram, A. Bers and L. Gauthier, *Phys. Fluids* 31:1614 (1988).

$$(K_1B')' - K_0B = \lambda F \qquad (3b)$$

where $' \equiv (d/d\xi)$. Associated with (3) is the power conservation equation

$$[\mathrm{Im}(F^*F' - B^*K_1B')]'$$

$$= -BB^*\ \mathrm{Im}K_0 - B'B^{*\prime}\ \mathrm{Im}K_1 \qquad (4)$$

Global conservation laws (i.e., connection formulae) are obtained from (4) upon integration and use of asymptotic WKB solutions.

We now note that F and B contain various spatial scales of variation. Away from the coupling region they can be represented by eikonal amplitudes accounting for the inhomogeneity in the magnetic field. In the coupling region they acquire an additional, slowly-varying amplitude due to coupling and dissipation. Separating these spatial evolution scales, we obtain CME's for the slowly-varying amplitudes (which we denote by f and b) due to coupling and dissipation; further, introducing a stationary phase expansion around the coupling point, the CME's are

$$f' = -i\lambda_c \exp[D_c - i\kappa(\xi - \xi_c)^2/2]b \qquad (5a)$$

$$b' = i\lambda_c \exp[-D_c + i\kappa(\xi - \xi_c)^2/2]f \qquad (5b)$$

where the stationary phase point ξ_c is given by

$$N_c^2 = N_B^2 \text{ with } N_c^2 = \lambda(1 + N_\parallel^2)/(1/3 + N_\parallel^2)$$

and

$$N_B^2 = -\mathrm{Re}(K_0/K_1);\ \lambda_c^2 = \lambda^2/4N_c^2K_{1c},$$

$$\kappa = c_A(1/3 + N_\parallel^2)/N_c\beta_1R_0\omega,$$

and

$$D_c = \int_{-\infty}^{\xi c} d\xi[\mathrm{Im}(K_0/K_1)]/2N_B$$

is the damping factor. Equations (5a) and (5b) give Weber's equation, whose asymptotics are well-known.

Thus, in high-field (HF) incidence of the FAW, we obtain the mode-conversion coefficient

$$C_{HF} = \frac{2\pi}{|\Lambda|} \frac{\exp(-\pi\,\mathrm{Re}\Lambda - 2D_c)}{|\Gamma(-i\Lambda)|^2} \qquad (6)$$

where $\Lambda = \lambda_c^2/\kappa$. The transmission coefficient is obtained as $T = \exp(-2\pi\,\mathrm{Re}\Lambda)$. In low-field (LF) incidence of the FAW, given the reflection coefficient R from the fast-wave approximation,[24] we obtain the mode-conversion coefficient

$$C_{LF} = (TR/C_{HF})\exp(-4D_c) \qquad (7)$$

In the absence of kinetic dissipation ($N_\parallel = 0$), equations (6) and (7) reduce to the well-known results: $C_{HF} = 1 - T$ and $C_{LF} = T(1 - T)$. Figures 6 and 7 give results obtained by our reduced order analysis for heating scenarios proposed in Alcator C-Mod and CIT.

ICRF Analytic Reduction Scheme For Nondegenerate Minority Heating

The analytic theory (see "Mode Conversion in the Presence of Kinetic Dissipation" on page 164) of dissipative coupling for ICRF, previously limited to D(H) minority heating,[25] has been extended to include the important case of D – T – ^{3}He heating for arbitrary concentration ratios. It was found that a straight forward finite-Larmor radius expansion of the dispersion tensor for D(^{3}He) heating does not reproduce the properties of the full 3 × 3 dispersion relation. A spurious resonance in the ion-Bernstein branch

[24] Ibid.

[25] V. Fuchs and A. Bers, *Phys. Fluids* 31:12 (1988).

appears between the fast Alfvén wave cut-off and the minority fundamental harmonic and an associated spurious propagating mode appears on the low field side. In the other heating scenarios, the spurious singularity occurs well outside of the coupling region and can be ignored. A method for removing the singularity and obtaining the correct fourth order dispersion relation was developed and used for D(^{3}He) heating. Excellent agreement with the results from the Imre-Weitzner boundary layer code is obtained.[26]

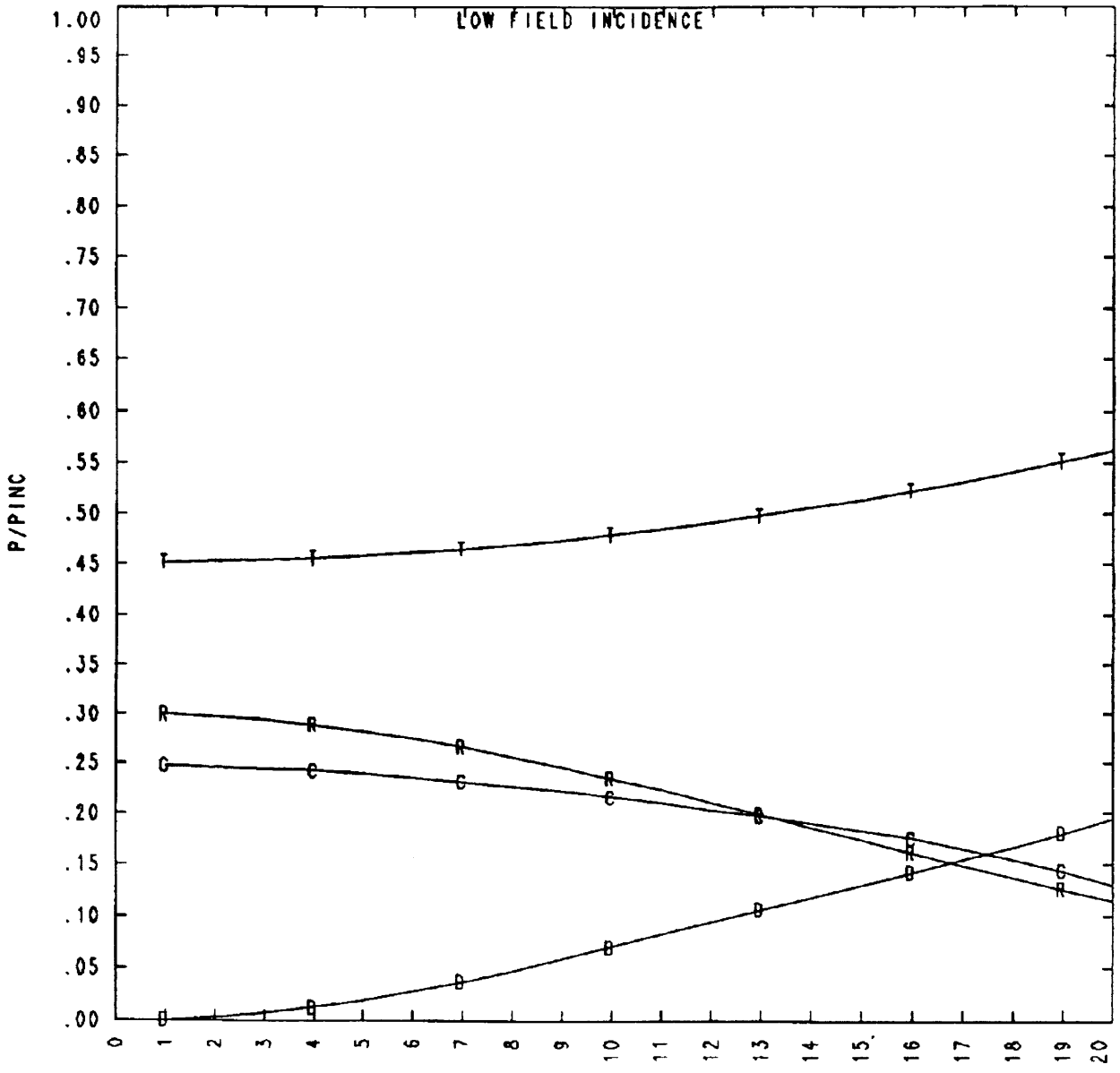

Figure 6. Power transfer coefficients T, R, C and the power dissipated, D, for low field incidence for Alcator C-Mod heating. $R_0 = 64$ cm, $f = 80$ MHz, $B_0 = 9$T, $T_0 = 2$ keV, $n_e = 5 \times 10^{20} m^{-3}$.

[26] K. Imre, Private communication

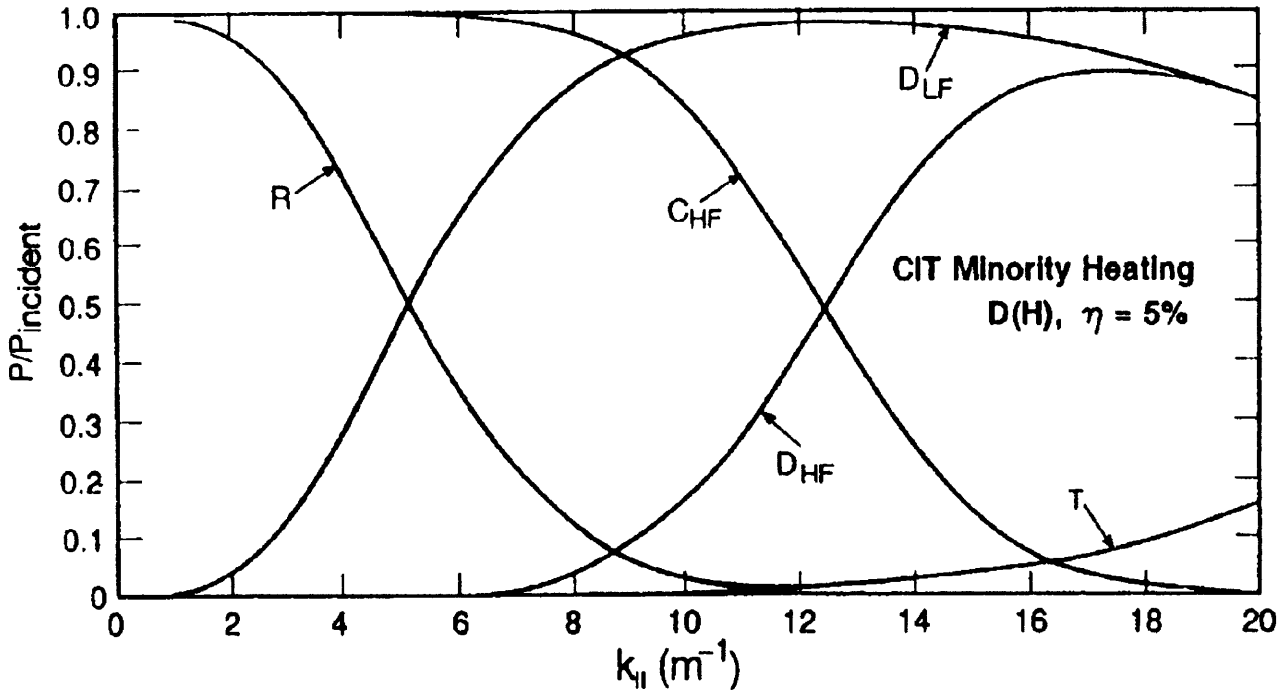

Figure 7. Power transfer coefficients T, R, $C_{HF}(C_{LF} < 0.01)$, and the powers dissipated, D_{HF} and D_{LF}, for CIT minority heating. $R_0 = 1.75$ m, f = 95 MHz, $B_0 = 7$T, $T_0 = 14$ keV, $n_e = 1.3 \times 10^{20} m^{-3}$, D(H), $\eta = 0.05$.

*A portion of this work was carried out in collaboration with members of the theory and computation group at the Tokamak de Varennes in Canada.

1.3 Physics of Thermonuclear Plasmas

Sponsor

U.S. Department of Energy
(Contract DE-AC02-78ET-51013)

Project Staff

Professor Bruno Coppi, Dr. Ronald C. Englade, Dr. Stefano Migliuolo, Dr. Linda Sugiyama, Paolo Detragiache, Ricardo Betti, Stefano Coda, Yi-Kang Pu

The main theme of this program is the theoretical study of magnetically confined plasmas in regimes of thermonuclear interest. A variety of physical regimes that fall in this category characterize both present-day experiments on toroidal plasmas (Alcator, TFTR, JET, etc.) as well as future ones that will contain ignited plasmas employing either first generation fuels, namely a deuterium-tritium mixture (Ignitor, CIT), or more advanced fuels such as deuterium-deuterium or deuterium-helium (Candor). A coordinated effort of collaboration between the design group of CIT, the U.S. compact ignition experiment, and the European Ignitor has been set up with our participation. At MIT, the Alcator C-Mod facility is under construction. This experiment combines the favorable features of elongated plasma cross sections with those of high field compact geometries. These features have been embodied earlier in both the Ignitor and the CIT designs, as well as in a machine (proposed by us in the early 1970's) called Megator. A recently proposed MIT program called Versator-Upgrade, has, as its main purpose, to achieve the "second stability" region for ideal MHD ballooning modes. We were the first group to discover this stability region in the winter of 1977-1978, and to outline the experimental procedure by which to reach it. This consists of starting with a

tight aspect ratio configuration, and raising the value of q (the inverse of the local rotational transform) on the magnetic axis above a certain level, such as 1.4, while increasing the value of the plasma pressure parameter, β_P, to those typical of the second stability region.

Presently, our research program follows two major avenues. First, the basic physical processes of thermonuclear plasmas (equilibrium, stability, transport, etc.) are being studied as they apply to existing or near-term future systems. In this effort, we closely collaborate with our experimental colleagues. Second, we explore advanced regimes of thermonuclear burning, including those employing low neutron yield fuels (D-^{3}He and "catalyzed" D-D). We consider both the design of machines to contain these ultra-high temperature plasmas as well as the physics that governs their behavior.

Below, we present some salient results on topics pursued by our group this past year, as well as from current research.

1.3.1 Anomalous Ion Thermal Conductivity

Over the past few years we have undertaken a comprehensive analytic and numerical study of the anomalous ion thermal transport associated with a microinstability known variously as the ion temperature gradient mode, η_i, or ion mixing mode. Many of the relevant properties of this mode were outlined by our group[27] as part of the analysis of the mechanism responsible for inward particle transport in toroidal devices. Subsequently, the increased energy confinement times τ_E and record values of the confinement parameter achieved by pellet injection[28] in Alcator C have validated our previously suggested[29] "cure," for the observed inadequate energy confinement times in the plasmas produced by Alcator C, that significant anomalous ion thermal conductivity could be avoided by producing peaked density profiles.

Our recent investigations focused on the spatial profile and parameter dependence of the mixing mode in toroidal devices. Simulations[30] successfully reproduced present day regimes and have been employed in predictions regarding high field experiments in ignited regimes. A collaborative effort has been initiated with scientists at Columbia University where a linear containment device is being built for the purpose of studying the threshold properties of the ion temperature gradient mode. Attention will be given to the effect of a non-uniform radial electric field on the stability properties of this mode.

1.3.2 Profile Consistency: Global and Nonlinear Transport

It is experimentally well established that the steady-state electron temperature profile in tokamak discharges is relatively independent of the spatial deposition of auxiliary power and assumes a canonical shape that can be related to that of a macroscopically stable and relaxed current density profile outside the region of sawtooth activity. This behavior is often referred to as the "principle of profile consistency."[31] In addition, localized heat pulse propagation is faster than the steady state transport for Ohmic discharges, but comparable for auxiliary heated discharges with flat deposition profiles.

---

[27] T. Antonsen, B. Coppi, and R. Englade, *Nucl. Fusion* 19:641 (1979).

[28] S. Wolfe et al., *Nucl. Fusion* 26:329 (1986).

[29] B. Coppi, In *Abstracts of the 1984 Annual Controlled Fusion Theory Conference,* Lawrence Livermore National Laboratory, Lake Tahoe, Nevada, 1984.

[30] R. Englade, RLE PTP-87/12 (1987), to appear in *Nucl. Fusion* (1989).

[31] B. Coppi, *Comm. Plasma Phys. Cont. Fusion* 5:261 (1980).

These considerations have led us to conclude[32] that the relevant electron cross-field heat flux is the result of at least two different transport processes described as fast and slow. The slow process can be appropriately described by a standard diffusion term that is linear in the temperature gradient, but the fast process is strongly determined by the departure of the electron temperature from the canonical profile and has a nonlinear temperature gradient dependence in our formulation. In neither case is the magnitude of transport required to explicitly depend on the profile and strength of the source of electron thermal energy, even though the solution of the energy balance equation adheres reasonably closely to the "principle of profile consistency." Analytic solutions of a simplified energy balance equation verify the applicability of the model.

1.3.3 Sawtooth and Fishbone Stabilization in Auxiliary Heated and Fusion Burning Plasmas

Recent experiments at JET[33] have shown that ion cyclotron resonance heating (ICRH) can stabilize "sawtooth" oscillations. Shortly after ICRH turn-off, a sawtooth crash occurs with a delay time that is a finite fraction of the slowing down time of energetic ions produced by the RF fields.[34] In collaboration with the JET theory group, we have undertaken a study of the interaction of global $n^\circ = 1, m^\circ \simeq 1$ internal modes (which are responsible for the sawtooth) with a high energy ion population. Standard MHD theory[35] yields an instability parameter for these internal modes, denoted λ_H. The energetic ions 1) contribute to a reduction in this parameter $\lambda_H \rightarrow \lambda_H + \mathrm{Re}(\lambda_K) < \lambda_H$, and 2) provide a viscous-like dissipation term, $\mathrm{Im}(\lambda_K)$ that arises from a resonance between the mode and trapped energetic ions that precess around the torus due to the curvature of the equilibrium magnetic field.

In high temperature plasmas, where finite ion diamagnetic frequency has brought the ideal $m^\circ \simeq 1$ kink to marginal stability, the residual growth is provided by electrical resistivity. This growth can be negated by hot ion effects. Detailed calculations, using a model distribution function appropriate for energetic ions produced by ion cyclotron resonance heating, have shown[36] that a finite window of stability exists in β_p -β_{ph} space (β_p = poloidal beta of thermal plasma, β_{ph} = poloidal beta of energetic particles) against all $m^\circ = 1$ internal modes and that, for a given q(r) profile, there exists a maximum value of the thermal plasma parameter $\lambda_H \propto \beta_p^2$ above which no stabilization is possible. We have also identified[37] the important role played by $\lambda_K(\omega = 0)$ on the stabilization of the resistive internal kink. These topics have been further considered in the context of ignited deuterium-tritium plasmas[38] where fusion α-particles are shown to stablize ideal modes that would otherwise produce "sharkstooth oscillations" of the central plasma column. By parametrizing the α -particle functional

$$\lambda_K = (r_o/R)^{3/2}\,(V_A/\sqrt{3}\,S_o R\omega_{D\alpha})\,\beta^*_{p\alpha}\,\Lambda_K(\omega/\omega_{D\alpha M})$$

where r_o is the position of the $q(r) = 1$ surface, S_0 the magnetic shear at that surface,

---

[32] B. Coppi, *Phys. Lett. A* 128:193 (1988).

[33] D.J. Campbell et al., *Phys. Rev. Lett.* 60:2148 (1988).

[34] F. Porcelli and F. Pegoraro, Second European Fusion Theory Meeting, Varenna, Italy, 1987.

[35] M.N. Bussac, R. Pellat, D. Edery, and J.L. Soule, *Phys. Rev. Lett.* 35:1638 (1975).

[36] B. Coppi, R.J. Hastie, S. Migliuolo, F. Pegoraro, F. Porcelli, *Phys. Lett. A*132:267 (1988).

[37] F. Pegararo, F. Porcelli, B. Coppi, P. Detragiache, S. Migliuolo, in *Plasma Physics and Controlled Nuclear Fusion Research 1988.* International Atomic Energy Agency (1989). Forthcoming.

[38] B. Coppi, S. Migliuolo, F. Pegoraro, F. Porcelli, submitted to *Phys. Fluids* (1989).

V_A the Alfvén frequency, $\omega_{D\alpha M}$ a representative[39] value of the precession drift frequency and $\beta^*_{p\alpha}$ the mean poloidal beta weighted by $(r/r_o)^{3/2}$, marginal stability can be expressed in terms of the almost universal curve $\Lambda_K(\omega/\omega_{D\alpha})$, a curve whose principal dependency is on the q(r) profile of the relevant experiment.

1.3.4 Density Limit and D-T ignition Conditions

Relatively high values of the plasma density are required to ensure a confinement parameter $n\tau_E$ (central electron density times energy confinement time) sufficient to reach ignition even for deuterium-tritium fuel. Collisional ion thermal conductivity and bremsstrahlung radiation, both proportional to the square of the particle density, play a strong role in the global energy balance up to temperatures somewhat above T_m, the "minimum ignition temperature." Near and above T_m, the presence of an anomalous ion thermal conductivity can have significant effects. Investigation of the microinstability known as the ion temperature gradient mode (also the η_i or ion mixing mode) shows that it can give rise to an ion thermal conductivity that scales as $nT_i^{3/2}$. In collaboration with W. Tang of the Princeton Plasma Physics Laboratory, we have analyzed an approximate model equation for the steady state energy balance in the central region of a tokamak plasma which includes this type of transport.[40] Multivalued solutions for the density are obtained as a function of temperature, ion thermal anomaly strength, and power.

If no ion anomaly is active, the density must remain below a certain maximum value for the plasma to attain the minimum ignition temperature T_m, but any density is allowed beyond T_m. In the presence of anomalous transport, a critical heating power deposition that increases with the magnitude of the anomaly is required to open a channel between regions of allowed density for temperatures above and below T_m. Since the rate of change of the fusion cross-section decreases with temperature, the density must be progressively increased above a minimal value, to heat the plasma to steady-state temperatures considerably higher than T_m.

1.3.5 Alpha Particle Induced Fishbone Oscillations in Fusion Burning Plasmas

The "fishbone" is a burst of oscillations that occurs in some experiments in which plasmas have two components, a main plasma and an energetic ion population. The fishbone has toroidal $n^\circ \simeq 1$ and poloidal $m^\circ \simeq 1$ spatial dependence and a frequency close to the diamagnetic frequency of the core (main plasma) ions.[41] Three requirements must be met to have instability: 1) high enough temperatures are produced so that finite diamagnetic frequency brings the ideal mode to marginal stability; 2) the core plasma beta must exceed a threshold value; and 3) a viscous-like resonant interaction of the wave with trapped energetic ions, that precess due to the curvature of the magnetic field, must exist. For parameters relevant to an Ignitor device,[42] alpha particles with energies near 300 keV resonate with the fishbone oscillation.

Recent work[43] has focused on the stabilization of this mode (as well as that of the internal kink, see 1.3.3, "Sawtooth and Fishbone Stabilization in Auxiliary Heated

---

[39] Ibid.

[40] B. Coppi and W.M. Tang, *Phys. Fluids* 31:2683 (1988).

[41] B. Coppi and F. Porcelli, *Phys. Rev. Lett.* 57:2272 (1986); B. Coppi, S. Migliuolo and F. Porcelli, *Phys. Fluids* 31:1630 (1988).

[42] B. Coppi, L. Lanzavecchia, and the Ignitor Design Group, *Comm. Plasma Phys. Cont. Nucl. Fusion* 11:47 (1987).

[43] B. Coppi, S. Migliuolo, F. Pegoraro, F. Porcelli, submitted to *Phys. Fluids* (1989); B. Coppi and F. Porcelli, *Fusion Technology* 13:447 (1988); B. Coppi, S. Migliuolo and F. Porcelli, RLE PTP-88/4 (1988).

and Fusion Burning Plasmas" on page 169) as a consequence of the energetic particle contribution, $\lambda_K(\omega)$, to the effective instability parameter $\lambda_H + \lambda_K(\omega)$. Here λ_H is the parameter given by standard[44] ideal MHD theory. The real part of λ_K is negative for modes with $\omega \simeq \omega_{di}$ much lower than $\omega_{D\alpha M}$ which is a measure of the precession drift frequency of alphas at their birth energy. Thus, the effective instability parameter decreases and the fishbone restabilizes at high enough α-particle pressure. This stabilization arises as the last step in the stabilization of the ideal internal kink (see 1.3.3, "Sawtooth and Fishbone Stabilization in Auxiliary Heated and Fusion Burning Plasmas" on page 169), namely when:

$$\sqrt{3}\, R\omega_{*i}/V_A \geq \lambda_H + Re\lambda_K(\omega) \geq 0$$

We have also found that another $m^\circ \simeq 1$ oscillation can exist, but only at very high α pressure ($\beta_{p\alpha} > 1$). This oscillation is at higher frequency ($\omega \gtrsim \omega_{D\alpha M}/3$) and can be entirely supported by trapped energetic ions which provide a destabilizing contribution: $Re[\lambda_K(\omega \gtrsim \omega_{D\alpha M}/3)] > 0$. This instability, now known as the "fast fishbone," was in fact discovered previously[45] in the context of fishbones observed in beam injected plasmas.

1.3.6 Transport Simulations of Thermonuclear Ignition in Compact Experiments

The attainment of ignition in a toroidal device depends critically on the net balance between bulk heating of the plasma and energy loss due mainly to anomalous electron and ion thermal conductivity, bremsstrahlung, synchrotron radiation, and macroscopic processes such as sawtooth oscillations. Using a modified version of the BALDUR one and one-half-dimensional transport code,[46] we have investigated the impact of these processes on the time evolution of D-T plasmas in a compact, high field device of the Ignitor type with strong ohmic heating.[47]

We have used a generalization of Coppi-Mazzucato-Gruber diffusion to model electron heat transport that includes the effects of alpha particle heating. For an anomalous ion heat diffusion coefficient peaked halfway out in the discharge and sawtooth repetition times down to 0.3 seconds, ohmic ignition could be achieved over a fairly wide density range. A central electron density near $8\ 10^{14} cm^{-3}$ was optimal in the sense of allowing relatively rapid approach to the state in which fusion heating dominates ohmic heating. A slightly higher density allows faster heating to fusion burning regimes. The overall magnitude of electron heat transport could be increased about a factor of two before ignition was prevented, while the magnitude of ion heat transport was not a sensitive parameter. In addition, we have studied the effects of variations in the form of electrical resistivity, plasma impurity level, and flux surface equilibrium configuration on the approach to ignition. Simulation of the Compact Ignition Tokamak (CIT) illustrates the rather strong auxiliary heating requirements of that design.

In collaboration with Miklos Porkolab, we have modified our one and one-half equilibrium and transport code to study electron cyclotron radio frequency heating prospects in the proposed CIT by incorporating power deposition results from a stand-alone ray tracing package. We have simulated some important aspects of proposed heating scenarios. We have examined the individual effects of electron and ion thermal diffusivity magnitudes, sawteeth, profile consistency,

---

[44] M.N. Bussac, R. Pellat, D. Edery, and J.L. Soule, *Phys. Rev. Lett.* 35:1638 (1975).

[45] L. Chen, R.B. White, M.N. Rosenbluth, *Phys. Rev. Lett.* 52:1122 (1984).

[46] G. Bateman, Spring College on Plasma Physics, Trieste, Italy, 1985.

[47] R. Englade, RLE PTP-87/12 (1987), to appear in Nucl. Fusion (1989).

and density profile shape in achieving ignition in this experiment.[48]

1.3.7 Experiment to Investigate D-^{3}He Burning

Recent developments in the design of high magnetic field toroidal experiments for the study of D-T burning plasmas have encouraged us to consider the possibility of an experiment burning D-^{3}He at higher temperatures and pressures. We have proposed a design, the Candor,[49] that can be constructed using present-day technology. It has a D-shaped cross section, with major radius $R_o = 170$ cm, a horizontal minor radius of 65 cm and a vertical elongation of 1.8. The vacuum toroidal magnetic field would reach up to 13.5 Tesla at R_o and the maximum toroidal plasma current would be 18 megamperes. The machine is intended to use D-T burning as the initial boost to reach D-^{3}He burning conditions. We are carrying out this work with several engineering and scientific groups in the United States and Europe.

1.3.8 Advanced Fuel Fusion

The strength of potentially damaging, high energy neutrons from the D-T fusion reaction makes other reactions, such as D-^{3}He and D-D, more attractive for a potential reactor. We have developed a set of numerical transport codes that can handle the multiple ion species (protons, deuterons, tritons, ^{3}He , ^{4}He) and have used the one-dimensional version to study the dynamics of ignition and burn for the Candor device.[50] Results show that ignition of D-^{3}He using a D-T start-up is possible if the thermal transport losses do not increase rapidly with temperature. Studies of the D-^{3}He burning state have shown that lean (i.e., 30 percent of the total ion density) ^{3}He mixtures will burn at the lowest values of the plasma beta (the ratio of the plasma kinetic to magnetic energies). Effective fusion ash removal and central fueling of the burning nuclei are essential to a sustainable reaction. Given these prerequisites, either burn control or operation at high beta are necessary because the low temperature burning state is dynamically unstable.

1.3.9 The Role of the Ubiquitous Mode in Anomalous Electron Energy Transport

Electron thermal energy transport in magnetically confined plasmas is one of the most important subjects in fusion research. Experiments indicate that such a transport process is anomalous, namely that the observed electron energy confinement time is an order of magnitude smaller than the one predicted by collisional neoclassical theory. We find[51] that the ubiquitous mode[52] satisfies the required[53] properties for driving the anomalous transport:

1. It is driven by the electron temperature gradient;
2. It is active over a significant portion of the plasma column and is not sharply reduced in regions of considerable collisionality ($\upsilon_e/\varepsilon\omega_{be} \lesssim 1$);
3. Its wavelength is long enough to produce substantial energy transport over a significant portion of the plasma;

---

[48] R. Englade et al., International Sherwood Theory Conference, San Antonio, Texas (1989).

[49] B. Coppi and L. Sugiyama, RLE PTP-88/6 (1988), submitted to *Nucl. Fusion*.

[50] Ibid.

[51] Y-K. Pu, Ph.D. diss., MIT, 1988.

[52] B. Coppi and F. Pegoraro, *Nuclear Fusion* 17:969 (1977).

[53] B. Coppi, *Phys. Lett. A* 128:193 (1988).

4. The energy transport is up to an order of magnitude larger than the corresponding particle transport.

1.4 Tokakmak Experiments in the High Poloidal Beta Regime on Versator II

Sponsors

U.S. Department of Energy
(Contract DE-AC02-78-ET-51013)

Project Staff

Professor Miklos Porkolab, Dr. Kuo-in Chen, Dr. Stanley C. Luckhardt, Stefano Coda, Jeffrey A. Colborn, Robert J. Kirkwood, Nora Nerses, Kurt A. Schroder, Jared P. Squire, Jesus N.S. Villasenor

In the past year, experiments on the Versator II tokamak have pioneered an experimental technique for producing plasma equilibria with very high values of poloidal beta. Poloidal beta (β_p) is defined as the ratio of the volume average plasma pressure to the magnetic pressure generated by the tokamak plasma current. In toroidal equilibria at high β_p instability of ideal MHD ballooning instabilities can limit the maximum achievable plasma pressure achievable in tokamaks. However, if these modes could be stabilized, a significant design constraint in tokamak D-T fusion reactors would be eliminated. Such high β_p operation is also an important step to making advanced fuel fusion reactors feasible.

Experiments have been carried out on Versator II in a regime of low plasma current with the aim of reaching high poloidal beta, β_p. These experiments use the energetic electron population created by lower hybrid current drive to provide the plasma current and a dominant component of the plasma pressure. The phenomena studied include toroidal equilibria at high β_p ($\varepsilon\beta_p \cong 1.3$), RF driven current profiles with high q(0), access to the second stability regime, and related magnetic and density fluctuation phenomena at high $\varepsilon\beta_p$.

Our experiments will address issues in the following areas: 1) MHD equilibrium properties of high β_p toroidal equilibria, 2) access to the second stability regime for ballooning modes, and 3) related fluctuations and instabilities at high β_p. At Versator II, we have pioneered a technique for producing such high $\varepsilon\beta_p$ plasmas that the pressure is predominantly generated by energetic electrons maintained by lower hybrid current drive. The energetic electron population created by RF current drive has an anisotropic pressure with $P_\parallel \gg P_\perp$ where

$$P_\parallel = \int d^3v[\gamma m_e f_e(v_\parallel, v_\perp)v_\parallel^2]$$

and

$$P_\perp = \int d^3v[\gamma m_e f(v_\parallel, v_\perp)v_\perp^2]$$

are the components of the pressure tensor parallel and perpendicular to the magnetic field. The poloidal beta for such an anisotropic pressure plasma entering the toroidal equilibrium condition was evaluated by Mondelli and Ott[54] to be

$$\beta_p = \frac{<1/2P_\parallel>}{B_a^2/2\mu_o} + \frac{<1/4P_\perp>}{B_a^2/2\mu_o} \qquad (1)$$

where the brackets indicate a toroidal volume average, and $B_a = \mu_o I/(2\pi a)$. (Note that $P_\perp$ as defined above contains v_ρ^2 and v_θ^2 terms.) The energetic electron velocity distribution function, $f(v_\parallel, v_\perp)$, generated by lower hybrid current drive, has been the subject of extensive theoretical work[55] and well founded analytical models of f are available.
Generally f(v) consists of a Maxwellian bulk and a flat plateau produced by quasilinear diffusion extending up to a maximum parallel velocity $v_\parallel = v_2$. Using the analytic model

[54] A. Mondelli and E. Ott, *Phys. Fluids* 17:1018 (1974).

[55] N.J. Fisch, *Rev. Modern Phys.* 59:175 (1987); V. Fuchs et al., *Phys. Fluids* 28:3619 (1985).

discussed in Fuchs et al.,[56] the above formula for β_p can be evaluated to give

$$\beta_p^{TAIL} = C_t \frac{I_A(v_2)}{I_{RF}} \qquad (2)$$

where I_{RF} is the RF driven plasma current; I_A is the Alfvén current, $I_A = 17\gamma v_2/c$ in kA; γ is the usual relativistic factor evaluated at $v = v_2$, and C_t is a model dependent numerical constant and is approximately equal to unity. Equation 2 indicates that high poloidal beta can be produced by reducing the RF current below the Alfvén current. Experiments on Versator II have demonstrated this effect as discussed in Luckhardt et al.[57] and provide a means of producing high poloidal beta toroidal equilibria in our experiment.

The following is a summary of the activities in the high $\varepsilon\beta_p$ experiments, theory and modeling of Versator II, diagnostics, and data analysis.

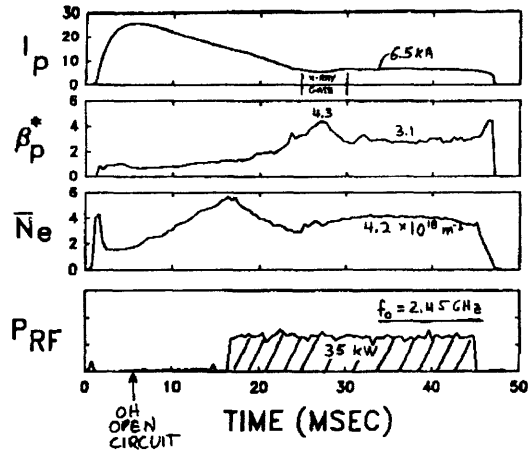

Figure 8.

1.4.1 High Poloidal Beta Using f = 2.45GHz Current Drive

During 1987, the high poloidal beta equlibrium technique was developed with current drive at f=0.8GHz. Recently these experiments were repeated using the f=2.45GHz RF system, allowing operation at higher density. A discharge obtained with the f=2.45GHz system is shown in figure 8. Note that $\beta_p + 1_i/2 \equiv \beta_p^*$ by definition. Operation at increased density improves the accuracy of the density measurement and simplifies the analysis of hard x-ray profile data.

1.4.2 New Magnetic Diagnostics Installed

An array of 36 poloidal magnetic field probes was constructed and installed and has been used in detailed magnetic equilibrium analysis (see 1.4.3, "Data Analysis with XFIT"). Further magnetic diagnostics have been designed for measurement of fast magnetic fluctuations associated with kink or possibly ballooning modes. These consist of magnetic probes to be installed inside the vacuum chamber. Two types of probes will be used; the first of which is a magnetic pickup coil designed for Alcator C-MOD. This probe is shown in figures 9 and 10. The frequency response of the coil has a bandwidth of $\cong$ 0.5MHz. The coil mount can be rotated to pick up fluctuations in both the toroidal and poloidal directions. A second type of pickup probe was designed which consists of a set of short length coils capable of detecting fluctuations with higher poloidal mode numbers (see figure 11). For $q_a = 27$ this array will detect modes with $m \leq 160$ and $n \leq 6$.

1.4.3 Data Analysis with XFIT

An equilibrium analysis code was developed similar to the EFIT code developed at GA

[56] V. Fuchs et al., *Phys. Fluids* 28:3619 (1985).

[57] S.C. Luckhardt et al., *Phys. Rev. Lett.* 62:1508 (1989).

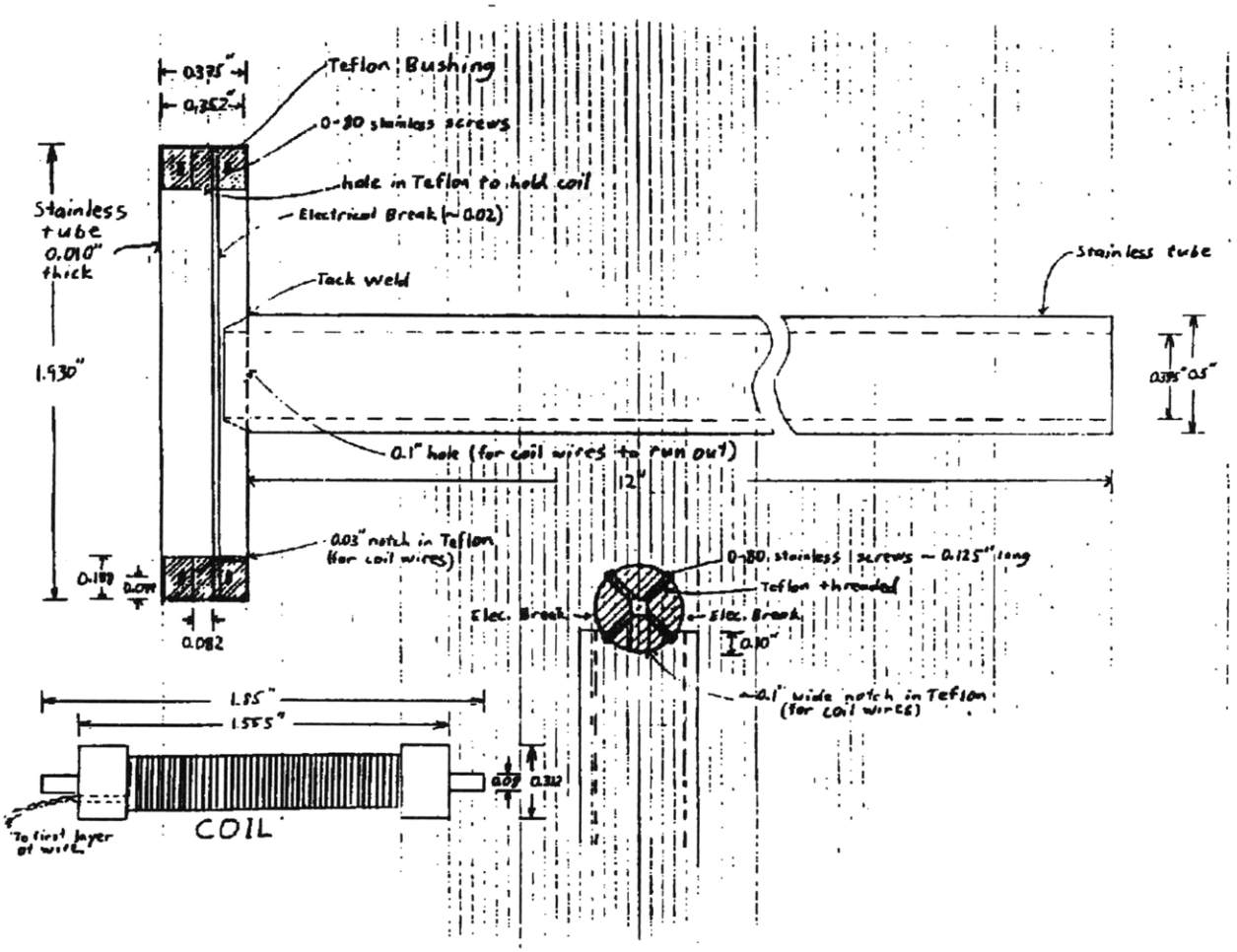

Figure 9.

Technologies.[58] In Versator experiments measurements of the x-ray emissivity profile using collimated PHA detectors provided crucial information about the width of the RF current profile. Current profile widths are much more difficult to obtain in ohmically driven plasmas and this width measurement in these experiments allows approximate values for 1_i and q(0) to be found.

A data analysis code, XFIT, was developed using PC-MATLAB software on an IBM PS/2 model 80 computer. XFIT includes equilibrium modeling of magnetic probe array data, density profile and hard x-ray profile data. The x-ray measurements in conjunction with the density profile give information about the current width allowing determination of the plasma internal inductance and approximate values for q(0). The code flow chart is shown in figure 12, and figure 13 shows an example of a best fit model equilibrium RF current profile, density profile, and x-ray emissivity profile. The results of this fitting procedure are values of 1_i, q(0), β_p, magnetic axis location, position and shape of the outer flux surface, and a best fit model MHD equilibrium with $J_\psi(r,z)$ and $\psi(r,z)$. Figure 14 shows the time evolution of the flux surfaces for the discharge shown in figure 8. Note that the current profile width is determined from x-ray and density profiles

[58] L.L. Lao et al., *Nucl. Fusion* 25:1611 (1985).

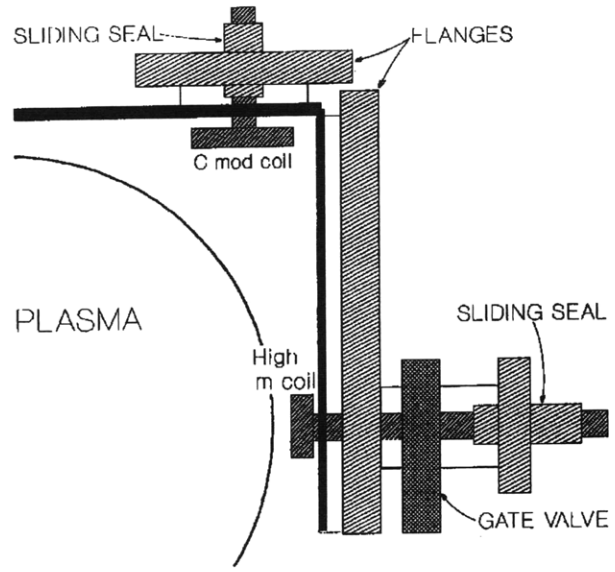

Figure 10. The test coils in the vacuum chamber.

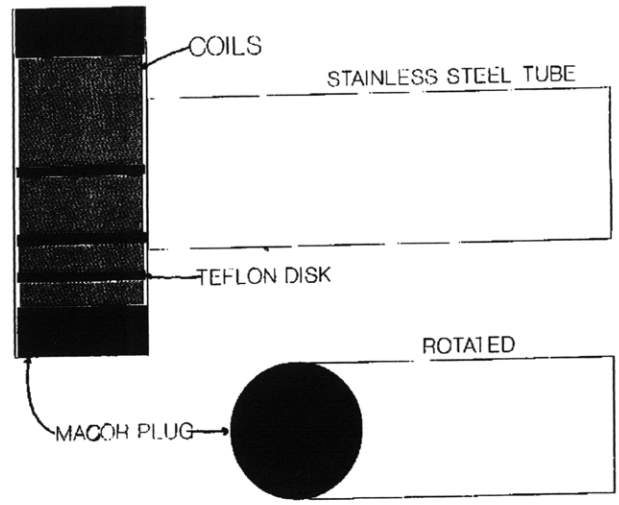

Figure 11. Design of the next test coil.

during the steady state RF-driven portion of the discharge. Current profile widths cannot be determined accurately during the initial ohmic inductive phase. This time sequence shows that the separatrix does not enter the limiter volume at the highest β_p, and, hence, these plasmas have not reached an equilibrium limit. Further, the outward motion of the plasma during the current ramp-down causes the current to continue to decay after the initiation of the RF pulse, but later in the sequence the equilibrium is seen to re-center and fill the volume to the limiter radius.

1.4.4 Comparison with High Poloidal Beta MHD Equilibrium Theory

The outward shift of the magnetic axis as a function of β_p for high poloidal beta toroidal equilibria has been calculated analytically by J. Friedberg[59] using model high β_p equilibria. In this series of experiments, the magnetic axis was compared to the observed outward shift of the density profile, and the magnetic probe array fit of the magnetic axis position. The observed shifts (see figure 15) were found in agreement with predictions of high $\varepsilon\beta_p$ equilibrium theory. This result provides confirmation of equilibrium theory at high $\varepsilon\beta_p$ where little or no data was available.

1.4.5 MHD Modeling and Criteria for Transition to the Second Stability Regime

Theoretical calculations were carried out by the PFC theory group including Drs. Jay Kesner, Barton Lane and Stefano Migliuolo. Regarding the ballooning mode stability condition for anisotropic pressure plasmas, they showed that when $P_\parallel \gg P_\perp$ the stability condition is the same as for a scalar pressure plasma ($P_\parallel \gg P_\perp$). This result suggests that the present experiments with anisotropic pressure are relevant indicators of possible future machines with high $\varepsilon\beta_p$ and scalar pressure.

With regard to transition to the second stability region: in the initial stage of these experiments we had begun using simple ana-

[59] J.P. Friedberg, *Rev. Mod. Phys.* 54:801 (1982).

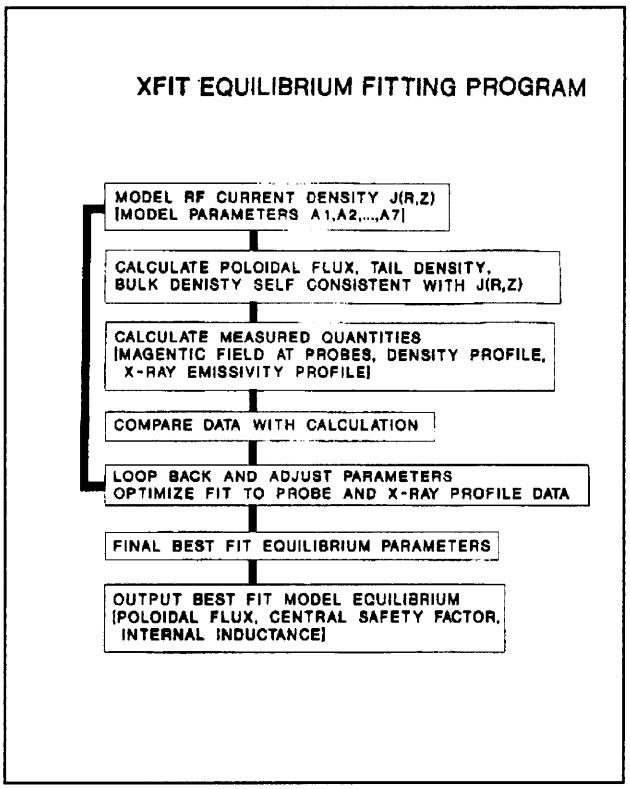

Figure 12.

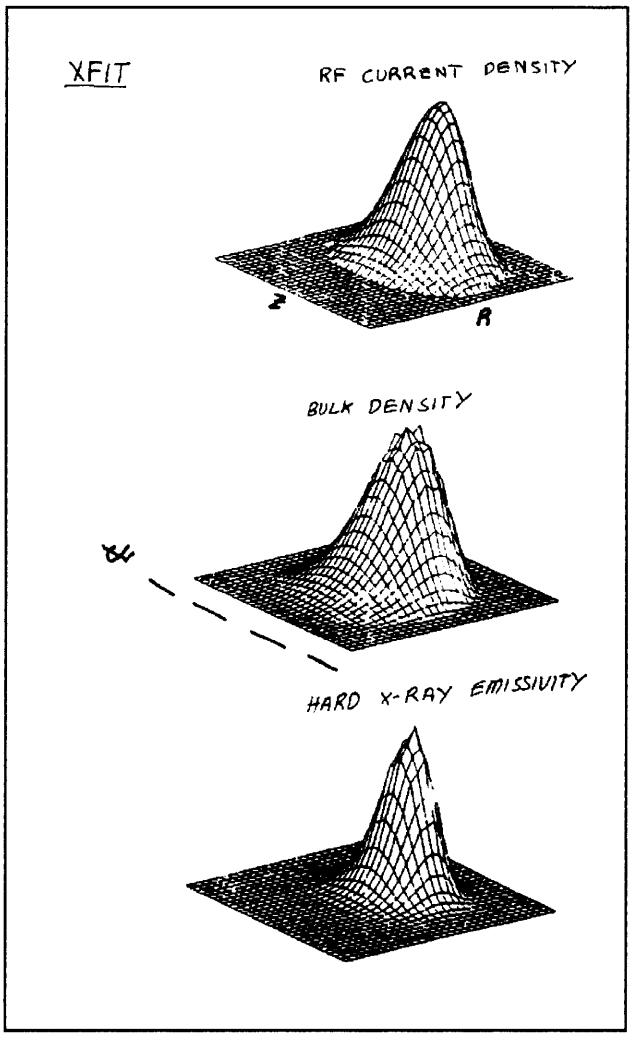

Figure 13.

lytical criteria available in the literature, e.g., the Troyon criterion, the Wesson Sykes condition, etc., to assess the stability of these equilibria. This analysis has been considerably improved in the past year. Now the predictions of ideal MHD equilibrium and stability theory modeling are obtained using the Princeton-Grumman PEST code. Model MHD equilibria were constructed which best fit the experimental equilibria as determined from XFIT. The model MHD equilibria were then tested for stability to high n ballooning modes using the PEST code. It was found that equilibria which best modeled the experiments had approximately circular plasma boundaries and values of q(0) ranging up to q(0)= 6. The numerical modeling found a stable transition from the first to the second regime when $q(0) > 5$, $q_a = 20$, and $\varepsilon\beta_p > 0.4$. Here we define the transition to second stability as occuring at the least stable or most unstable value of β_p. For lower q(0), higher q_a, or broader pressure profiles, an unstable range of $\varepsilon\beta_p$ exists for high n modes, but at higher $\varepsilon\beta_p$ these modes restabilize. For q(0) $\cong$ 6 (as indicated for these experiments by XFIT) and $q_a = 28$ these modes restabilized above $\varepsilon\beta_p$ = 0.7. Thus for $\varepsilon\beta_p > 0.7$ these plasmas are predicted to enter the second stable region. The experimental model equilibria were plotted on a stability diagram for high n ballooning modes and the result is shown in figure 16. The data points for the three equilibria at highest β_p appear to be in the second stability region. Thus, the code modeling of our experiment suggests that some of the equilibria obtained were near or beyond the transition to the second stability region.

These experiments have been reported in *Physical Review Letters* 62:3 (1989) and presented in an invited talk at the 1988 APS Division of Plasma Physics Meeting in Hollywood, Florida. The magnetic flux surface reconstruction was first presented at the IAEA TCM on Research Using Small Tokamaks on October 10, 1988, in Nice, France, and a paper on these results will be

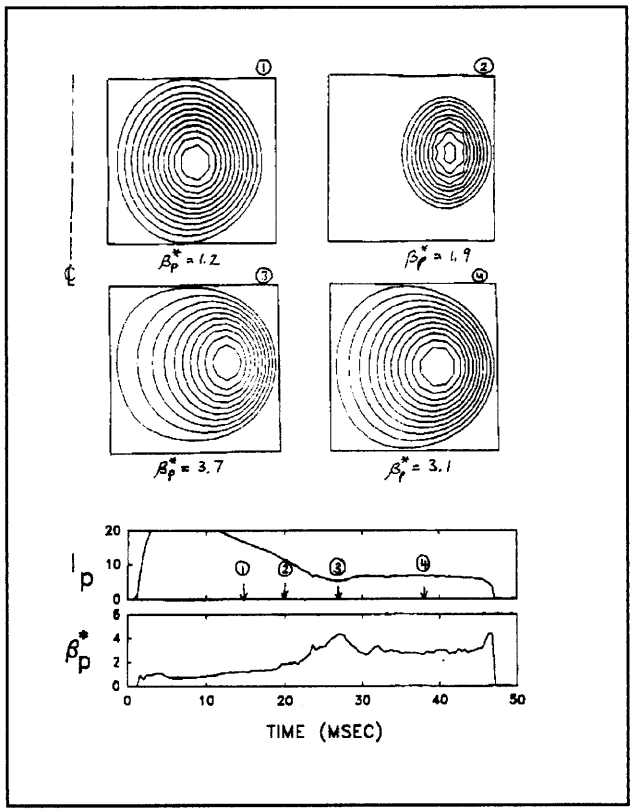

Figure 14.

published in the proceedings of that meeting. Another paper containing the experimental results and theory contributions was presented at the 12th International Conference on Plasma Physics and Controlled Fusion in Nice, France (1988). The results of experiments using the 2.45GHz current drive system to produce high β_p plasmas were presented at the U.S./Japan Workshop on Advanced Current Drive Methods at Kyoto University, Kyoto, Japan (1988), and a paper will appear in the proceedings of that workshop.

The equilibrium characteristics of these high β_p plasmas has been the subject of the bulk of the experimental work to date. The ballooning mode stability of these equilibria has been assessed by MHD code modeling. Taking into account information on the current profile width coming from the x-ray profile measurement, the important parameters 1_i and q(0) are known to some degree. Although the theoretical modeling of these plasmas suggests that the second stability regime was entered, it is desirable to find more experimental evidence that this is indeed the case. In the coming year, we plan to improve our x-ray and density profile diagnostics, and install diagnostics to look for ballooning mode activity in these plasmas.

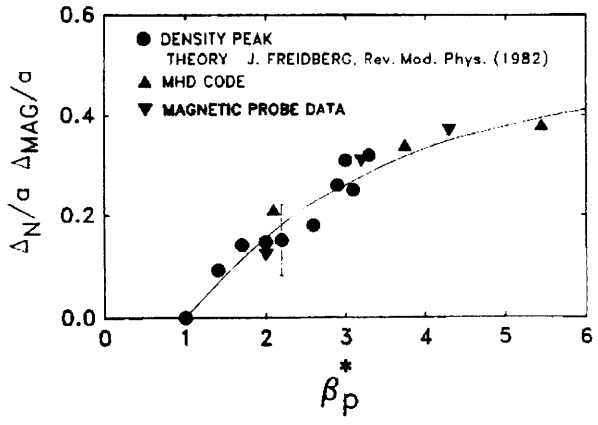

Figure 15.

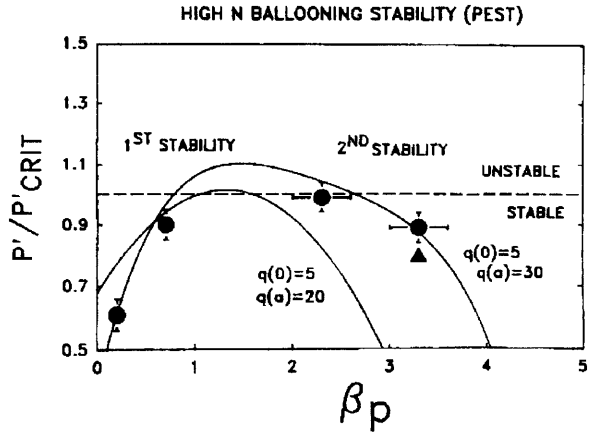

Figure 16.